

Two Homometallic Antiferromagnets Based on Oxalato-Bridged Honeycomb Assemblies: $(A)_2[M^{II}_2(C_2O_4)_3]$ (A = Ammonium Salt Derived from Diethylenetriamine; $M^{II} = Fe^{2+}, Co^{2+}$)

Zhiming Duan,^{†,‡} Yan Zhang,[§] Bin Zhang,^{*,†} and Francis L. Pratt^{*,||}

BNLMS, Organic Solid Laboratory, CMS & Institute of Chemistry, Chinese Academy of Sciences, Beijing, 100190, P. R. China, Graduate School, Chinese Academy of Sciences, Beijing, 100049, P. R. China, Department of Physics, Peking University, Beijing, 100871, P. R. China, and ISIS, Rutherford Appleton Laboratory, Chilton, Didcot, OX11 0QX, United Kingdom

Received November 2, 2008

Oxalato-bridged divalent homometallic compounds $A_2[M^{II}_2(C_2O_4)_3]$ ($M^{II} = Fe^{2+}$ (**1**), Co^{2+} (**2**)) were obtained by a solvothermal method. They consist of honeycomb anions and cations, that is, the 5-oxo-1,4,7-triazabicyclo[4.3.0]non-6-en-7-yl ammonium ion (hereafter abbreviated as A_1) in **1** and the 2-(2,3-dioxo-1-piperazinyl)eth-1-yl ammonium ion (hereafter abbreviated as A_2) in **2**, which were generated from in situ reactions of diethylenetriamine (DETA) with oxalic acid catalyzed by the metal ions and yielded two compounds with different cell parameters: $a = 17.2224(4)\text{Å}$, $b = 9.3151(2)\text{Å}$, $c = 15.1518(4)\text{Å}$, $\beta = 95.767(1)^\circ$, $V = 2418.5(1)\text{Å}^3$, and $Z = 4$, $C2/c$ for **1** and $a = 9.6924(2)\text{Å}$, $b = 15.8325(4)\text{Å}$, $c = 17.2995(4)\text{Å}$, $\beta = 95.144(1)^\circ$, $V = 2644.0(1)\text{Å}^3$, $Z = 4$, and $P2_1/n$ for **2**. A_1 points its carbonyl group to the pocket of the honeycomb network. A_2 forms a helical chain around the anion layers through hydrogen bonds along the 2_1 axis, and the crystal remains achiral due to the existence of the inversion symmetry. The methanol molecules occupy the holes situated between A_2 and the oxalate network in **2**. The distance between two anion layers in **1** was shorter than in **2** due to the template effect of the ammonium salts. In the anion layers, the hexagonal rings are elongated along the a axis in **1** and **2**. There are interactions as hydrogen bonds between the cation and anion and between cations. A broad maximum observed in the temperature-dependent susceptibility curve shows antiferromagnetic interactions between paramagnetic ions. The antiferromagnetic ordering at 28 K in **1** and 21 K in **2** was confirmed by ac susceptibility and specific heat measurements. Hysteresis loops with a coercive field of 17 Oe in **1** and 2300 Oe in **2** were observed at 2 K.

Introduction

Over the past decades, there has been increasing interest in hybrid molecule-based magnets. In these compounds, two or more different molecular fragments are used to construct the network structure and exhibit the magnetic properties. One of the most used molecular fragments is the short connector oxalate ion ($C_2O_4^{2-}$, ox).¹ Its versatile abilities in coordinating metal ions and mediating efficient magnetic coupling among magnetic metal sites have allowed the

construction of various molecular materials, including magnetic metal–ox frameworks of different dimensionalities (1D–3D) showing rich magnetism and dual-functional materials such as magnetic conductors and superconductors as well as magneto-optical compounds.^{2–6} More recently, we demonstrated an antiferromagnetic neutral zigzag chain

* To whom correspondence should be addressed. Phone: 86 (China)-10-62558982(B.Z.), 44(United Kingdom)-1235-445135(F.P.). Fax: 8610(China)-62559373 (B. Z.), 44(United Kingdom)-1235-446881 (F.P.). E-mail: zhangbin@iccas.ac.cn (B.Z.), francis.pratt@stfc.ac.uk (F.P.).

[†] CMS & Institute of Chemistry, Chinese Academy of Sciences.

[‡] Graduate School, Chinese Academy of Sciences.

[§] Peking University.

^{||} Rutherford Appleton Laboratory.

(1) (a) Decurtins, S.; Pellaux, R.; Antorrena, G.; Palacio, F. *Coord. Chem. Rev.* **1999**, *192*, 841. (b) Clément, R.; Decurtins, S.; Gruselle, M.; Train, C. *Monatsh. Chem.* **2003**, *134*, 117. (c) Miller, J. S. *Molecular Magnet*, VI; 2005. (d) Wang, X. Y.; Wang, Z. M.; Gao, S. *Chem. Commun.* **2008**, 281.

(2) (a) Hursthouse, M. B.; Light, M. E.; Price, D. J. *Angew. Chem., Int. Ed.* **2004**, *43*, 472. (b) Li, L. L.; Lin, K.; Ho, C. J.; Sun, C. P.; Yang, H. D. *Chem. Commun.* **2006**, 1286. (c) Coronado, E.; Galan-Mascaros, J. R.; Marti-Gastaldo, C. *J. Am. Chem. Soc.* **2008**, *130*, 14987.

(3) Tamaki, H.; Zhang, Z. J.; Matusmoto, N.; Kida, S.; Koikawa, M.; Achiwa, N.; Hashimoto, Y.; Okawa, H. *J. Am. Chem. Soc.* **1992**, *114*, 6974.

oxalate compound with long-range magnetic ordering at 10.7 K and a weak ferromagnetic, neutral, layered oxalate compound with long-range magnetic ordering at 23 K.⁷ We have aimed to find new magnetic units for dual-functional molecular crystals combining conductivity and magnetism using similar units to the 1D chain magnetic anion $[\text{Fe}(\text{C}_2\text{O}_4)\text{Cl}_2]_n^-$ that has already produced examples of a weak-ferromagnetic insulator, semiconductor, and conductor.^{5a,b,8}

Bimetallic oxalate-bridged anions $[\text{MM}'(\text{C}_2\text{O}_4)_3]_n^-$, such as $[\text{M}(\text{Cr}(\text{C}_2\text{O}_4)_3)_n]^-$ ($\text{M} = \text{Mn}^{2+}, \text{Fe}^{2+}, \text{Co}^{2+}, \text{Ni}^{2+}, \text{Cu}^{2+}, \text{Zn}^{2+}$) for ferromagnets, $[\text{Mn}_3(\text{H}_2\text{O})_4\{\text{Cr}(\text{C}_2\text{O}_4)_2\}_3]_n^{3-}$, $[\text{Mn}(\text{CH}_3\text{OH})\text{Cr}(\text{C}_2\text{O}_4)_3]_n^-$, and ferrimagnets $[\text{M}^{\text{II}}\text{Fe}^{\text{III}}(\text{C}_2\text{O}_4)_3]_n^-$ ($\text{M} = \text{Mn}^{2+}, \text{Fe}^{2+}$), which are composed of honeycomb anion layers and organic counteranions, have been intensively studied due to their novel and intriguing magnetic behavior.^{3,9} Two strategies have been adopted in the construction of such systems from solution: one is by varying the paramagnetic transition metal ions from divalent M^{II} to trivalent M^{III} , leading to ferri- or ferromagnetic bulk properties. At the beginning of the 1990s, Okawa et al. first reported the two-dimensional heterometallic ferromagnet.³

From then on, enormous efforts have been made toward two-dimensional heterometallic magnets.⁹ Relatively few examples of two-dimensional homometallic ferrimagnets have been obtained, and in these systems, the valence states of two metal ions are mixed, such as $[\text{Fe}^{\text{II}}\text{Fe}^{\text{III}}(\text{C}_2\text{O}_4)_3]_n^-$.¹⁰ However, examples of two-dimensional homometallic anions $[\text{M}^{\text{II}}_2(\text{C}_2\text{O}_4)_3]_n^{2-}$ have been rarely reported so far.¹¹ Therefore, there will be a need for a comparison of the properties of homometallic compounds with different ground states and heterometallic compounds with the same ground state, such as $(n\text{-C}_5\text{H}_{11})_4\text{N}[\text{Mn}^{\text{II}}\text{Fe}^{\text{III}}(\text{C}_2\text{O}_4)_3]$, where the two metal ions have the $[\text{Ar}]3d^5$ electronic configuration and ${}^6\text{A}_1$ ground state.^{9b}

The other strategy is to vary the counteranions. The counteranions cannot only be changed from electronically, optically, or magnetically inactive ternary or quaternary ammonium salts to electro-, opto-, or magneto-active species such as TTF, stilbazolium-shaped chromophores, $[\text{M}(\text{sal}_2\text{trien})]^+$ ($\text{M} = \text{Fe}^{3+}, \text{In}^{3+}$), decamethylmetallocenium cations, organic radicals, and crown-ether in dual-function molecular crystals^{3,5} but also act as templates controlling the formation of the net structure. For example, when $[\text{M}^{\text{II}}(\text{bpy})_3]$ was used as a cation, a 3D oxalate network was obtained in both homometallic ($[\text{Mn}_2(\text{C}_2\text{O}_4)_3]_n^{2-}$, $[\text{Fe}_2(\text{C}_2\text{O}_4)_3]_n^{2-}$, and $[\text{Co}_2(\text{C}_2\text{O}_4)_3]_n^{2-}$) and heterometallic ($[\text{M}^{\text{II}}\text{Cr}^{\text{III}}(\text{C}_2\text{O}_4)_3]_n^-$ and $[\text{M}^{\text{II}}\text{Fe}^{\text{III}}(\text{C}_2\text{O}_4)_3]_n^-$) compounds.¹² When bulky ammonium cations were used, they intercalated into the honeycomb anion layers, and the interlayer separation varied from 8.5 to 17.5 Å, depending on the size of the cations.^{3,9–11} Tuning of the interlayer separation of the network by the ternary or quaternary ammonium salts may have an influence on the packing of the two-dimensional structures, and the use of novel organic amines may contribute to the formation of novel networks through versatile modes of short contacts. The simple structural ammonium salts can be replaced by the salts of linear or cyclic polyamines; thus, subtle tuning of the interlayer separation can be achieved by multiple short contacts which exist at the nitrogen sites of the polyamines.

On the basis of the above considerations, we intended to understand the template effect of diethylenetriamine (DETA) in the formation of oxalate-bridged compounds, as was observed in the formate and phosphate compounds with polyamines.¹³ The neutral zigzag chain antiferromagnet $\text{Co}(\text{C}_2\text{O}_4)(\text{HO}(\text{CH}_2)_3\text{OH})$ and layered antiferromagnet Fe -

- (4) (a) Hernandez-Molina, M.; Lloret, F.; Ruiz-Perez, C.; Julve, M. *Inorg. Chem.* **1998**, *37*, 4131. (b) Armentano, D.; Munno, G. D.; Mastropietro, T. F.; Lloret, G.; Julve, M. *Chem. Commun.* **2004**, 1160. (c) Armentano, D.; Munno, G. D.; Mastropietro, T. F.; Julve, M.; Lloret, F. *J. Am. Chem. Soc.* **2005**, *127*, 10778.
- (5) (a) Wang, X. H.; Ge, C. S.; Xing, X. C.; Wang, P.; Zhang, D. M.; Wu, P. J.; Zhu, D. B. *Synth. Metal.* **1991**, *39*, 355. (b) Wang, P.; Bandow, S.; Maruyama, Y.; Wang, X. H.; Zhu, D. B. *Synth. Metal.* **1991**, *44*, 147. (c) Kurmoo, M.; Graham, A. W.; Day, P.; Coles, S. J.; Hursthouse, M. B.; Caulfield, J. L.; Singleton, J.; Pratt, F. L.; Hayes, W.; Ducasse, L.; Guionneau, P. *J. Am. Chem. Soc.* **1995**, *117*, 12209. (d) Coronado, E.; Galan-Mascaros, J. R.; Gimenez-Saiz, C.; Gomez-Garcia, C. J.; Ruiz, P. C.; Triki, S. *Adv. Mater.* **1996**, *9*, 737. (e) Coronado, E.; Galan-Mascaros, J. R.; Gomez-Garcia, C. J.; Martinez-Agudo, M. *Adv. Mater.* **1999**, *11*, 558. (f) Coronado, E.; Galan-Mascaros, J. R.; Gomez-Garcia, C. J.; Laukhin, V. *Nature* **2000**, *408*, 447. (g) Ballester, G.; Coronado, E.; Gimenez-Saiz, C.; Romero, F. M. *Angew. Chem., Int. Ed.* **2001**, *40*, 792. (h) Alberola, A.; Coronado, E.; Galan-Mascaros, J. R.; Gimenez-Saiz, C.; Gomez-Garcia, C. J. *J. Am. Chem. Soc.* **2003**, *125*, 10774. (i) Coronado, E.; Galan-Mascaros, J. R.; Marti-Gastaldo, C. *Inorg. Chem.* **2006**, *45*, 1882.
- (6) (a) Cariati, E.; Macchi, R.; Roberto, D.; Ugo, R.; Galli, S.; Casati, N.; Macchi, P.; Sironi, A.; Bogani, L.; Caneschi, A.; Gatteschi, D. *J. Am. Chem. Soc.* **2007**, *129*, 9410. (b) Train, C.; Gheorghie, R.; Krstic, V.; Chamoreau, L.; Ovanesyanyan, N. S.; Rikken, G. L.; Gruselle, M.; Verdager, M. *Nat. Mater.* **2008**, *7*, 729.
- (7) (a) Zhang, B.; Zhang, Y.; Zhang, J. B.; Li, J. C.; Zhu, D. B. *Dalton Trans.* **2008**, 5037. (b) Duan, Z. M.; Zhang, Y.; Zhang, B.; Zhu, D. B. *Inorg. Chem.* **2008**, *47*, 9152.
- (8) (a) Zhang, B.; Wang, Z. M.; Fujiwara, H.; Kobayashi, H.; Inoue, K.; Kurmoo, M.; Mori, T.; Gao, S.; Zhang, Y.; Zhu, D. B. *Adv. Mater.* **2005**, *17*, 1988. (b) Zhang, B.; Wang, Z. M.; Zhang, Y.; Takahashi, K.; Okano, Y.; Cui, H.; Kobayashi, H.; Inoue, K.; Kurmoo, M.; Pratt, F. L.; Zhu, D. B. *Inorg. Chem.* **2006**, *45*, 3275. (c) Xu, H. B.; Wang, Z. M.; Liu, T.; Gao, S. *Inorg. Chem.* **2007**, *46*, 3089.
- (9) (a) Atovmyan, L. O.; Shilov, G. V.; Lyubovskaya, R. N.; Zhilyaeva, E. I.; Ovanesyanyan, N. S.; Pirumova, S. I.; Gusakovskaya, I. G.; Morozov, Y. G. *JETP Lett.* **1993**, *58*, 766. (b) Decurtins, S.; Schmalte, H. W.; Oswald, H. R.; Linden, A.; Ensling, J.; Gutlich, P.; Hauser, A. *Inorg. Chim. Acta* **1994**, *216*, 65. (c) Mathoniere, C.; Nuttal, C. J.; Carling, S. G.; Day, P. *Inorg. Chem.* **1996**, *35*, 1201. (d) Carling, S. G.; Mathoniere, C.; Day, P.; Malik, K. M. A.; Coles, S. J.; Hursthouse, M. B. *J. Chem. Soc., Dalton Trans.* **1996**, 1839. (e) Pelloux, R.; Schmalte, H. W.; Huber, R.; Fischer, P.; Hauss, T.; Ouladdiaf, B.; Decurtins, S. *Inorg. Chem.* **1997**, *36*, 2301. (f) Watts, I. D.; Carling, S. G.; Day, P. *Dalton Trans.* **2000**, 1429. (g) Coronado, E.; Galan-Mascaros, J. R.; Gomez-Garcia, C.; Ensling, J.; Gutlich, P. *Chem.—Eur. J.* **2000**, *6*, 552. (h) Coronado, E.; Galan-Mascaros, J. R.; Marti-Gastaldo, C.; Martinez, A. M. *Dalton Trans.* **2006**, 3294. (i) Clemente-Leon, M.; Coronado, E.; Dias, J. C.; Soriano-Portillo, A.; Willett, R. *Inorg. Chem.* **2008**, *47*, 6458.

- (10) Mathoniere, C.; Carling, S. G.; Dou, Y. S.; Day, P. *J. Chem. Soc., Chem. Commun.* **1994**, 1551.
- (11) Clemente-Leon, M.; Coronado, E.; Gimenez-Lopez, M. C.; Soriano-Portillo, A.; Waerenborgh, J. C.; Delgado, F. S.; Ruiz-Perez, C. *Inorg. Chem.* **2008**, *47*, 9111.
- (12) (a) Decurtins, S.; Schmalte, H. W.; Schneuwly, P.; Oswald, H. R. *Inorg. Chem.* **1993**, *32*, 1888. (b) Decurtins, S.; Schmalte, H. W.; Schneuwly, P.; Ensling, J.; Gutlich, P. *J. Am. Chem. Soc.* **1994**, *116*, 9521. (c) Hernandez-Molina, M.; Lloret, F.; Ruiz-Perez, C.; Julve, M. *Inorg. Chem.* **1998**, *37*, 4131. (d) Coronado, E.; Galan-Mascaros, J. R.; Gomez-Garcia, C. J.; Martinez-Agudo, J. M. *Inorg. Chem.* **2001**, *40*, 113. (e) Clemente-Leon, M.; Coronado, E.; Gomez-Garcia, C. J.; Sorai-Portillo, A. *Inorg. Chem.* **2006**, *45*, 5653.
- (13) (a) Wang, Z. M.; Zhang, B.; Fujiwara, H.; Kobayashi, H.; Kurmoo, M. *Chem. Commun.* **2004**, 47. (b) Wang, Z. M.; Zhang, X. Y.; Batten, S. T.; Kurmoo, M.; Gao, S. *Inorg. Chem.* **2007**, *46*, 8439. (c) Yang, Y. C.; Hung, L.; Wang, S. L. *Chem. Mater.* **2005**, *17*, 2833.

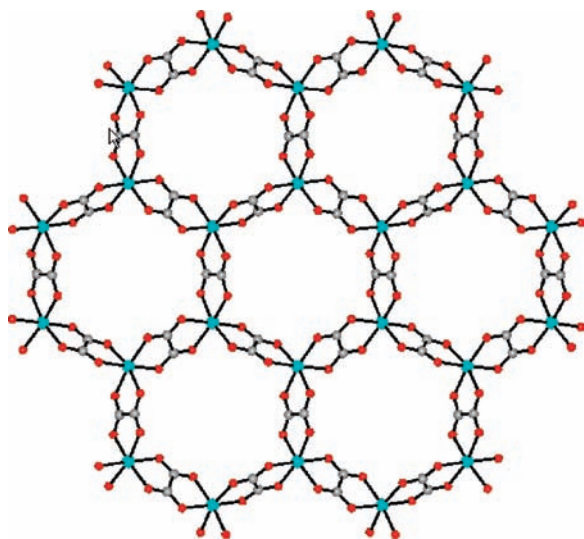


Figure 1. Anion layer in **1** and **2** projected onto the *ab* plane. Atomic scheme: metal ion, blue; C, gray; O, red.

(C₂O₄)(CH₃OH) were obtained from 1,3-propanediol and methanol under solvothermal conditions without a cation template.⁷ We hoped we could obtain a new coordination polymer which was different from Fe(C₂O₄)(CH₃OH) when DETA was used as the cation template.^{7a} We found that diethylenetriamine in situ reacted with oxalic acid to give new cyclic polyamines with the catalysis of the metal ions, and a class of divalent homometallic honeycomb anion layers was produced. Herein, we present the synthesis, structural features, and physical properties of these two-dimensional compounds.

Experimental Section

All reagents are commercially available and used as received without further purification unless otherwise stated. A mixture of 0.25 mmol of FeCl₂·4H₂O or CoCl₂·6H₂O, 1.50 mmol of H₂C₂O₄·2H₂O, 0.60 mmol of DETA, and 8 mL of methanol were sealed in a Teflon-lined stainless steel vessel, heated to 120 °C for 10 days under autogenous pressure, and then cooled to room temperature. The resulting crystals were collected and washed with methanol and then dried in the air at ambient temperature.

The orange rhombus-faceted crystal (A₁)₂[Fe₂(C₂O₄)₃] (**1**) was obtained with a yield of about 83%. Elem anal. (%) calcd for C₁₈H₂₀N₆O₁₄Fe₂ (656.07): C, 32.95; H, 3.07; N, 12.81. Found: C, 32.76; H, 3.33; N, 12.72. FT-IR (ν , cm⁻¹): 789, 796, 1619, 1659, 1697, 1726 for C=O; 1315, 1360 for C=C; 2889, 2922, 3001, 3120, 3213 for C–H and N–H. The crystal remains stable up to 270 °C.

The purple rhombus-faceted crystal (A₂)₂[Co₂(C₂O₄)₃]·CH₃OH (**2**) was obtained with a yield of about 87%. Elem anal. (%) calcd for C₁₉H₂₈N₆O₁₇Co₂ (730.32): C, 31.25; H, 3.86; N, 11.51. Found: C, 30.98; H, 3.70; N, 11.74. FT-IR (ν , cm⁻¹): 795, 1613, 1660, 1681, 1711 for C=O; 1315, 1363 for C=C; 2948, 3066, 3130, 3222 for C–H and N–H. The crystal remains stable up to 280 °C.

X-ray diffraction data of **1** and **2** were collected at 290 K on a Nonius Kappa CCD diffractometer with graphite monochromated Mo K α (λ = 0.71073 Å) radiation. Lorentz, polarization, and empirical absorption corrections were carried out.¹⁴ The crystal structure was solved by the direct method and refined by full-matrix

Table 1. Crystallographic Data of **1** and **2**

	1	2
formula	C ₁₈ H ₂₀ Fe ₂ N ₆ O ₁₄	C _{19.5} H ₂₄ Co ₂ N ₆ O ₁₆
fw	656.10	716.30
F(000)	1336	1460
T, K	293	293
cryst syst	monoclinic	monoclinic
space group	C2/c	P2 ₁ /n
<i>a</i> , Å	17.2224(4)	9.6924(2)
<i>b</i> , Å	9.3151(2)	15.8325(4)
<i>c</i> , Å	15.1518(4)	17.2995(4)
β , deg	95.767(1)	95.144(1)
<i>V</i> , Å ³	2418.5(1)	2644.0(1)
Z	4	4
<i>D</i> _{calcd} , g/cm ³	1.802	1.799
μ (Mo K α), mm ⁻¹	1.285	1.346
cryst size, mm ³	0.16 × 0.08 × 0.07	0.10 × 0.10 × 0.10
<i>T</i> _{min} , <i>T</i> _{max}	0.839, 0.922	0.803, 0.875
θ _{min} , θ _{max} , deg	3.59, 27.51	3.47, 27.47
no. total refls.	21408	39813
no. unique refls (<i>R</i> _{int})	2784(0.0633)	6045(0.0776)
no. obs. [<i>I</i> ≥ 2 σ (<i>I</i> ₀)]	1708	3662
no. params	221	490
R1, wR2 [<i>I</i> ≥ 2 σ (<i>I</i> ₀)]	0.0299, 0.0623	0.0392, 0.0822
R1, wR2 (all data)	0.0694, 0.0700	0.0870, 0.0936
GOF	0.913	0.951
^a $\Delta\rho$, e/Å ³	0.250, -0.265	0.407, -0.527
^b max. and mean Δ/σ	0.000, 0.000	0.001, 0.000
CCDC	699038	699039

^a Max and min residual density. ^b Max and mean shift/ σ .

least-squares on *F*² using the SHELX program, with anisotropic thermal parameters for all non-hydrogen atoms.¹⁵ Crystallographic data and refinement parameters are summarized in Table 1, and two structures have been deposited at the Cambridge Crystallographic Data Centre (CCDC 699038 for **1** and CCDC 699039 for **2**).

Magnetization measurements were performed on polycrystalline samples tightly packed into a capsule using a Quantum Design MPMS 5XL SQUID and a Quantum Design MPMS 7XL SQUID system. Susceptibility data were corrected for diamagnetism of the sample using Pascal constants (−116 × 10⁻⁶ cm³ mol⁻¹ for **1** and −106.5 × 10⁻⁶ cm³ mol⁻¹ for **2** per metal ion) and were corrected for the background through experimental measurement on the sample holder.¹⁶ Specific heat measurements were carried out on a Quantum Design PPMS 9XL system for a polycrystalline sample fixed onto the sample holder by N-grease. The data were corrected for the contribution of N-grease and the sample holder.

Results and Discussion

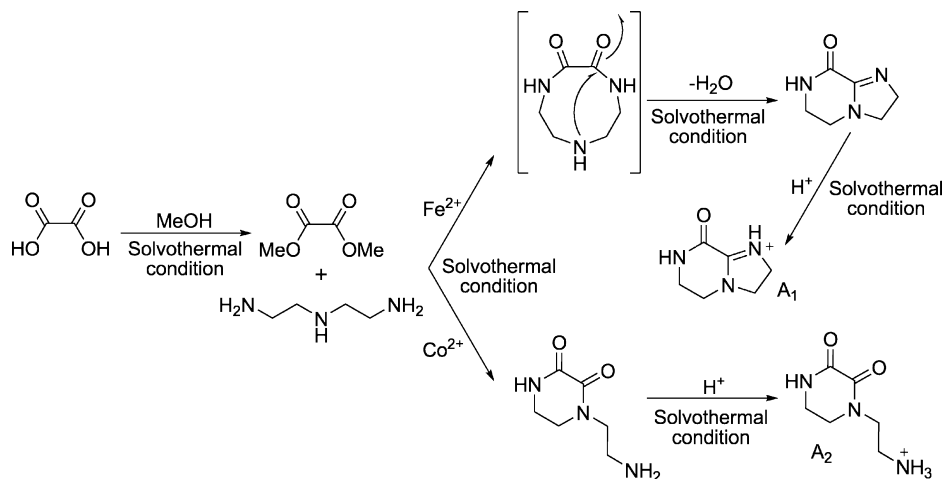
Synthesis. Hydrothermal and solvothermal reactions have been extensively applied to the synthesis of inorganic–organic hybrid materials, and in situ metal/ligand reactions under hydrothermal/solvothermal conditions have aroused great attention due to the structural novelty and unique properties for potential applications resulting from the versatile or even unconventional ligand synthesis.¹⁷ We selected solvothermal conditions for the synthesis of new oxalated-bridged molecular magnets such as Co(C₂O₄)(HO(CH₂)₃OH) and Fe(C₂O₄)(CH₃OH)⁷ and conducted the reaction in methanol at 120 °C for 10 days with relatively high and reproducible yields greater than 80%.

(15) Sheldrick, G. M. *SHELXL-97*; University of Göttingen: Göttingen, Germany, 1997.

(16) Kahn, O. *Molecular Magnet*; Wiley-VCH: Weinheim, Germany, 1993.

(17) (a) Zhang, X. M. *Coord. Chem. Rev.* **2005**, *249*, 1201. (b) Chen, X.-M.; Tong, M.-L. *Acc. Chem. Res.* **2007**, *40*, 162.

Scheme 1. Possible Route for the Formation of the New Organic Counterions



The crystals of **1** and **2** are coordination compounds consisting of oxalate-bridged honeycomb anions, as shown in Figure 1, and organic counterions with formulas of $(A_n)_2[M^{II}_2(C_2O_4)_3]$. The organic counterion was in situ synthesized from diethylenetriamine and oxalic acid under solvothermal conditions. The X-ray crystal structures show that diethylenetriamine has undergone intermolecular cyclic condensation with oxalic acid to form new organic counteranions. The high dilution reaction between diethylenetriamine and diethyl oxalate has previously been reported in the preferential synthesis of bicyclic polyamine.¹⁸ Hence, the condensation can occur in superheated methanol. As shown in Scheme 1, we suggested that oxalic acid first transformed into diethyl oxalate under superheated conditions, and then the resultant ester further reacted with diethylenetriamine to form two kinds of cyclic polyamines. A bicyclic compound formed readily in the presence of Fe^{2+} , while a monocyclic compound was formed preferentially in the presence of Co^{2+} . The monocyclic compound cannot be obtained by a direct method, although it has been successfully prepared through multistep Gabriel synthesis. The metal ion plays a catalytic role in the process of cyclic formation.^{17,19}

When the experiment was carried out without DETA under the same conditions, the coordination polymer $M(C_2O_4)(CH_3OH)$ ($M = Fe, Co$) was obtained. $M(C_2O_4)(CH_3OH)$ is a neutral 2D antiferromagnet with a [4,4] net.^{7a} So the cations derived from diethylenetriamine work as a template for the honeycomb anion under solvothermal conditions. This shows a new way to obtain oxalate-bridged honeycomb anions distinct from the previously reported room-temperature solution method.^{3,5,9}

Crystal Structure. Complex **1** crystallizes in the monoclinic space group $C2/c$. As shown in Figure 2, a 2D honeycomb anion layer of $[Fe_2(C_2O_4)_3]^{2-}$ is propagated within the ab plane. The cation layer contains one crystallographically independent A_1 cation. A pair of A_1 cations

related by the inversion symmetry operation are arranged alternately along the ab plane. One of the A_1 cations points its carbonyl group toward the pocket of the honeycomb network and the other toward the pocket of the neighboring layer, as shown in Figure 2. The dihedral angle between the main planes of the cation and the honeycomb anion layer is $62.20(5)^\circ$, and the dihedral angle between the main planes of two cations in one layer is $55.19(4)^\circ$. The long axis of the cation is almost parallel to the anion layer, so the separation distance between two anion layers is shorter than the reported ones at 7.58 \AA . There are a number of hydrogen

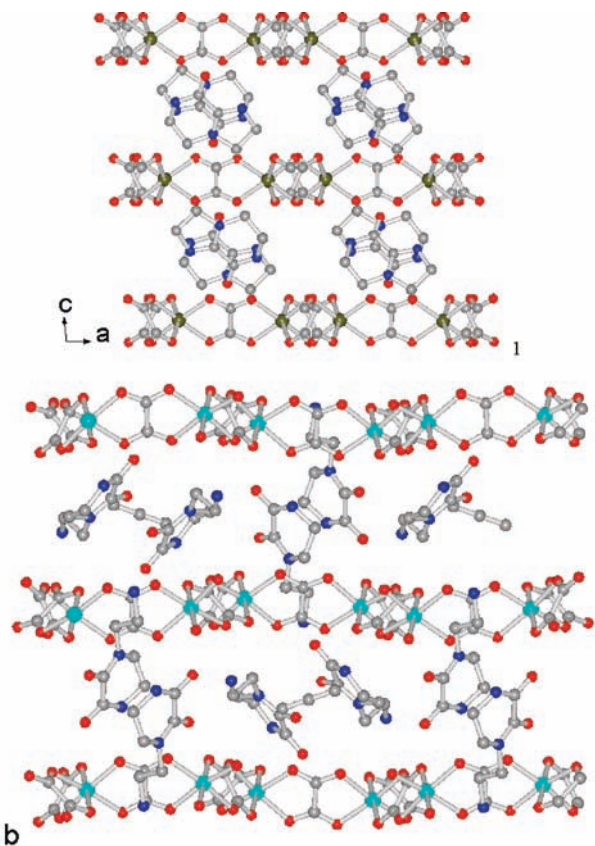


Figure 2. The packing diagram of **1** (top) and **2** (bottom) along the c direction, viewed along the b axis. Fe, green; Co, light blue; C, gray; O, red; N, blue. H atoms are not included.

(18) (a) Hori, T.; Momonoi, K.; Kiba, Y.; Yoshida, C.; Sakai, H.; Takeno, R.; Ohashi, T.; Kishimoto, S.; Saikawa, I. *Yakugaku Zasshi* **1979**, *99*, 730. (b) Creaser, S. P.; Lincoln, S. F.; Pyke, S. M. *J. Chem. Soc., Perkin Trans.* **1999**, *2*, 121.

(19) Hagrman, P. J.; Hagrman, D.; Zubieta, J. *Angew. Chem., Int. Ed.* **1999**, *38*, 2638.

bonds between cations and anions, N1–H1···O2 (2.819 Å/166°), N3–H10···O6 (2.756 Å/172°), C6–H5···O4 (3.324 Å/144°), and between anions, C7–H6···O7 (3.124 Å/131°).

Complex **2** crystallizes in the monoclinic space group $P2_1/n$. As shown in Figure 2, the 2D honeycomb anion layer of $[\text{Co}_2(\text{C}_2\text{O}_4)_3]^{2-}$ is extended across the ab plane. There are two crystallographically independent A_2 cations and one and a half methanol molecules in a cation layer. The chemical environments of two crystallographically independent A_2 cations are different. One is approximately parallel to the anion layer; the other intercalates its alkylamino group into the pocket of the honeycomb network. Two A_2 cations in neighboring cation layers are connected through hydrogen bonds between the carbonyl groups and the amino groups, N3–H10···O15 (2.84 Å/128°), N3–H10···O16 (2.85 Å/147°), N6–H22···O13 (2.74 Å/150°), N6–H22···O14 (2.93 Å/118°), C13–H15···O16 (3.51 Å/150°), C15–H18···O13 (3.14 Å/132°), C15–H19···O16 (2.75 Å/102°), and hydrogen bonds inside A_2 , C9–H7···O14 (2.72 Å/101°) and C15–H19···O16 (2.75 Å/102°). Therefore, the cations related by the 2_1 screw axis connect head-to-tail to form two independent helical chains which interlock the honeycomb rings running along the b axis (Figure S4, Supporting Information). The crystal is achiral because the chirality of the cation chains on neighboring layers is opposite. There are hydrogen bonds between the nitrogen of the cations and the oxygen in the anion layers, N1–H1···O11 (2.96 Å/170°), N3–H12···O6 (2.77 Å/169°), N4–H13···O12 (2.94 Å/174°), N6–H23···O2 (2.99 Å/164°), N6–H24···O3 (2.93 Å/160°), C8–H4···O4 (3.46 Å/1157°), C8–H5···O5 (3.35 Å/139°), C14–H16···O5 (3.34 Å/143°), and C14–H17···O8 (3.31 Å/138°). The methanol molecules occupy the holes situated between A_2 and the oxalate network.

As shown in Figure 1, both **1** and **2** contain oxalate-bridged homometallic honeycomb anion layers $[\text{M}_2^{\text{II}}(\text{C}_2\text{O}_4)_3]^{2-}$, which have been observed in heterometallic compounds such as $[\text{CrMn}(\text{C}_2\text{O}_4)_3]^-$ and $[\text{MnFe}(\text{C}_2\text{O}_4)_3]^-$ and homometallic ones such as $[\text{Fe}^{\text{II}}\text{Fe}^{\text{III}}(\text{C}_2\text{O}_4)_3]^-$, $[\text{Mn}^{\text{II}}_2(\text{C}_2\text{O}_4)_3]^{2-}$, $[\text{Zn}^{\text{II}}_2(\text{C}_2\text{O}_4)_3]^{2-}$.^{3,9–11,20} The distance between two neighboring anion layers' ranges is 7.58 Å for **1** to 8.65 Å for **2**, due to the intercalation of the counterions; this is in the same range as reported for honeycomb compounds. In the anion layers, the metal ion was octahedrally coordinated with six oxygen atoms from three oxalate anions with M–O distances of 2.119(1)–2.151(1) Å in **1**, 2.070(2)–2.145(2) Å in **2** and cis O–M–O angles of 78.2–99.3° in **1** and 78.9–103.8° in **2**. These values fall into the range for oxalate-bridged honeycomb anions of Fe^{II} and Co^{II} .^{9a,12} The hexagonal rings are slightly elongated along the a axis in both **1** and **2**, which can be explained by the presence of metal ions with the same electronic ground state in networks as observed in $[\text{Mn}_2^{\text{II}}(\text{Ox})_3]^{2-}$.¹¹

On the basis of the above-mentioned structural features, we consider that the ammonium salts of polyamines can act

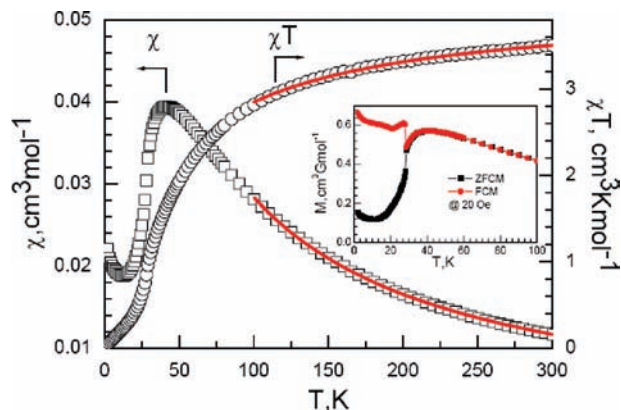


Figure 3. χ vs T and χT vs T plots of compound **1** under an applied field of 500 Oe. The red solid line represents the theoretical fits in the high-temperature region. Inset: ZFCM/FCM plots under 20 Oe in the low-temperature region.

as good templates for controlling the formation of the 2D honeycomb anion layers, as occurs in $[(S)\text{-}[\text{PhCH}(\text{CH}_3)\text{-N}(\text{CH}_3)_3]][\text{Mn}(\text{CH}_3\text{CN})_{2/3}\text{Cr}(\text{C}_2\text{O}_4)_3]\text{CH}_3\text{CN}$.^{9i,19}

Magnetic Properties. Given the structural features of the 2D extended honeycomb anion $[\text{M}_2^{\text{II}}(\text{C}_2\text{O}_4)_3]^{2-}$, a long-range ordering magnetization is expected, as observed in oxalate-bridged honeycomb compounds.

Complex 1. Under an applied magnetic field of 500 Oe, the temperature dependence of χ (Figure 3) displays a broad maximum around 40 K, a minimum at 28.1 K, and a further rise below 28 K. The broad maximum at 40 K corresponds to the low-dimensional antiferromagnetic interactions. At 300 K, the χT value was $3.5 \text{ cm}^3 \text{ K mol}^{-1}$, which is the same as the expected value ($3.5 \text{ cm}^3 \text{ K mol}^{-1}$) for the isolated, spin-only octahedral ion with $S = 2$ and $g = 2.00$. The χT value decreases continuously upon temperature lowering and shows a kink point at 28.1 K, corresponding to the quick rise below 28.1 K in the χ versus T plot, as shown in Figure 3. The susceptibility data above 100 K are well-fitted to the Curie–Weiss law with $R = 2.60 \times 10^{-7}$, giving Curie and Weiss constants of $C = 4.22 \text{ cm}^3 \text{ K mol}^{-1}$ and $\theta = -53 \text{ K}$. The large, negative Weiss temperature indicates a strong antiferromagnetic interaction between the Fe^{II} ions. Zero-field-cooled (ZFC) and field-cooled (FC) magnetization under 20 Oe show the irreversibility at 28.1 K, and FC magnetization values are small around 2 K (Figure 3, inset). The magnetization value in the ZFC and FC modes jumps rapidly at 28.1 K, which is similar to that observed in $S = 5/2$ heterometallic antiferromagnets such as $\text{N}(\text{-}C_5\text{H}_{11})_4\text{-MnFe}(\text{C}_2\text{O}_4)_3$ and $\text{RPPPh}_3\text{MnFe}(\text{C}_2\text{O}_4)_3$ ($R = C_3\text{H}_7, C_4\text{H}_9, C_5\text{H}_{11}, C_6\text{H}_{13}, C_7\text{H}_{15}$), and can be attributed to the onset of long-range antiferromagnetic ordering accompanied by spin canting.^{9d,g,21} The isothermal magnetization at 2 K displays a linear increase with increasing field and reaches $0.20 \text{ N}\beta$ at 60 kOe (Figure 4). The magnetic hysteresis loop shows values of coercive field (H_c) and remnant magnetization (M_r) of 17 Oe and $0.00007 \text{ N}\beta$, respectively. From the expected

(20) Vaidhyanathan, R.; Natarajan, S.; Rao, C. N. R. *Dalton Trans.* **2001**, 699.

(21) Bhattacharjee, A.; Gutlich, P. *J. Mag. Mag. Mater.* **2004**, 268, 380.

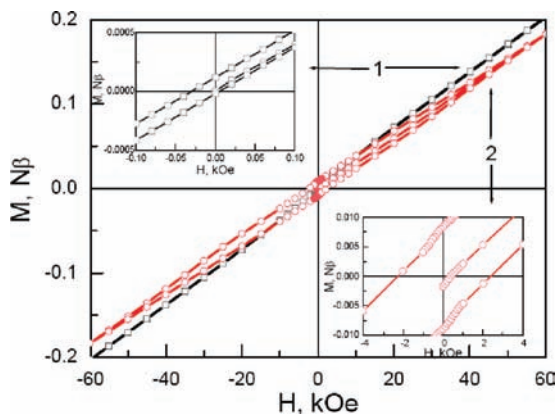


Figure 4. Isothermal magnetization of **1** (black square) and **2** (red circle) at 2 K. It reaches $0.20 N\beta$ at 60 kOe and about $0.23 N\beta$ at 70 kOe for **1** and $0.18 N\beta$ at 60 kOe for **2**. Inset: (left top) the low field of 100 Oe for **1**; (right bottom) the low field of 4000 Oe for **2**, a hysteresis at about 2300 Oe was observed.

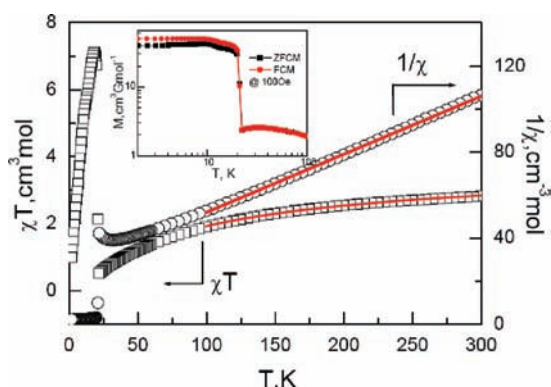


Figure 5. χT vs T and $1/\chi$ vs T plots for compound **2** under an applied field of 100 Oe. Red solid lines are fits to the Curie–Weiss law. Inset: ZFCM/FCM plots under 100 Oe in the low-temperature region.

saturation value of the magnetization for spin $S = 2$ ($4 N\beta$), a canting angle of 0.001° was assigned.

Complex 2. The temperature dependence of χ under an applied magnetic field of 100 Oe (Figure 5) displays a broad maximum at 30 K, a minimum at 21 K, and further a quick rise below 21 K. ZFC and FC magnetization under 100 Oe show the irreversibility below 21.0 K (inset of Figure 4). At 300 K, the χT value is $2.82 \text{ cm}^3 \text{ K mol}^{-1}$, which is the same as the observed value ($2.80 \text{ cm}^3 \text{ K mol}^{-1}$) in the antiferromagnetic chain compound $\text{Co}(\text{C}_2\text{O}_4)(\text{HO}(\text{C}_3\text{H}_6)\text{OH})$ and larger than the expected value ($1.875 \text{ cm}^3 \text{ K mol}^{-1}$) for the isolated, spin-only ion with $S = 3/2$ and $g = 2.00$.^{7b} This is expected for the Co^{2+} ion, owing to the significant orbital contribution of the Co^{2+} ion with strong spin–orbit coupling in an octahedral environment.²² The χT value decreases continuously upon lowering the temperature and shows a kink at 21 K, corresponding to the quick rise below 21 K in the χ versus T plot, as shown in Figure 5. The susceptibility data above 100 K are well-fitted to the Curie–Weiss law with $R = 3.49 \times 10^{-6}$, giving Curie and Weiss constants of $C = 3.70 \text{ cm}^3 \text{ K mol}^{-1}$ and $\theta = -92.1 \text{ K}$. The Weiss temperature indicates the strong antiferromagnetic interaction between Co^{2+} ions and the spin–orbit coupling of Co^{2+} . The

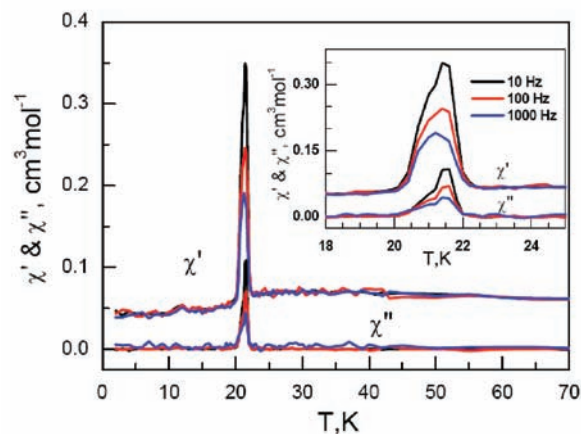
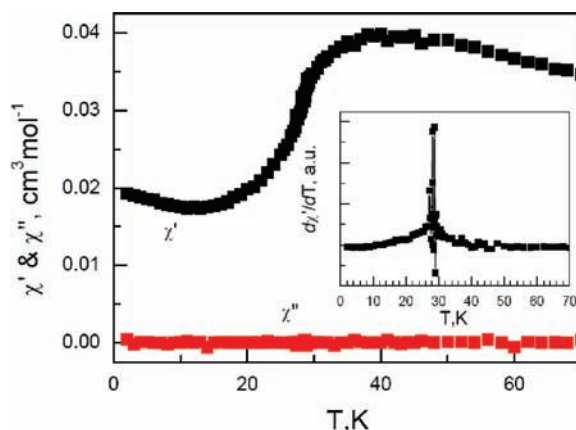


Figure 6. Temperature dependence of ac susceptibility measured with an ac of 2 Oe amplitude and 10 Hz oscillating frequency in a zero dc field for **1**. Inset: derivative $d\chi'/dT$ (top). Temperature dependence of ac susceptibility measured with an ac of 2 Oe amplitude and 10 Hz, 100 Hz, and 1000 Hz oscillating frequency in a zero dc field for **2**. Inset: expansion of the 18–25 K region. (bottom).

isothermal magnetization at 2 K (Figure 4) increases with increasing field and reaches $0.18 N\beta$ at 60 kOe. The magnetic hysteresis loop shows values of coercive field (H_c) and remnant magnetization (M_r) of 2300 Oe and $0.0087 N\beta$. From the expected saturation value of the magnetization for spin $S = 3/2$ ($3 N\beta$), a canting angle of 0.17° was assigned. These experiments confirmed that spin-canted antiferromagnetic long-range ordering (LRO) occurred in **1** and **2**.

The antiferromagnetic LRO in **1** and **2** was further confirmed by alternating-current (ac) susceptibility (Figure 6) and specific heat measurements in zero field (Figure S5, Supporting Information). The ac response of **1** was weak; no peak was found for both χ' and χ'' data. A kink was observed at 28 K in the χ' versus T plot, as clearly shown in the $d\chi'/dT$ plot. The ac response of **2** was stronger than that of **1**; there is a sharp peak observed around 21 K for both χ' and χ'' data. No frequency dependence of the temperature-dependent features was observed in both crystals between 10, 100, and 1000 Hz. In the primary specific heat measurement, a λ -shaped peak was observed at 28 K for **1** and at 21 K for **2**. These data clearly reveal the occurrence of magnetic LRO and agree with the previous magnetic studies.

Compared with the magnetic behavior of heterometallic and homometallic honeycomb compounds, we found that not only the electronic ground state of the metal ion but also

(22) Carlin, R. L.; van Duijneyeldt, A. L. *Magnetic Properties of Transition Metal Compounds*; Springer-Verlag: New York, 1977; pp 69.

the interactions between cations and anions via hydrogen bonds and the separation between anion layers play an important role in tuning the magnetic properties of the crystals. Experiments on other polyamines and transition metal ions are in progress.

Conclusion

Two divalent homometallic oxalate-bridged honeycomb compounds, $A_2M^{II}_2(C_2O_4)_3$ ($M^{II} = Fe^{2+}$ (**1**), Co^{2+} (**2**)), were obtained by a solvothermal method. The ammonium cations were in situ synthesized by the reaction of diethylenetriamine with oxalic acid under the catalysis of Fe^{II} and Co^{II} separately. The ammonium cations intercalate into the anion layers with extensive hydrogen bonds between not only the

cation and anion but also between cations in **1** and **2**. Both of these are antiferromagnets.

Acknowledgment. The authors thank Prof. Zheming Wang, Prof. Fuhui Liao, and Prof. Song Gao of College of Chemistry and Molecular Engineering, Peking University, for their kind help in X-ray experiment and magnetic measurements and for valuable discussions. This work was supported by CMS-CX200809, NSFC (No. 20673120, 20873154), and MOST 2006CB601001, 2006CB932102 of China.

Supporting Information Available: Additional figures and cif files. This material is available free of charge via the Internet at <http://pubs.acs.org>.

IC8021003